Radial correlation reflectometry analysis of tritium-rich and hybrid JET plasmas

A. Figueiredo[1], M. Maslov[2], C.D. Challis[2], C. Giroud[2], J. Hobirk[3], A. Kappatou[3], D.B. King[2], E. Lerche[4], JET contributors[5], and the EUROfusion Tokamak Exploitation Team[6]

[1] *IPFN, Instituto Superior Técnico, Universidade de Lisboa, 1049-001 Lisboa, Portugal*
[2] *UKAEA, Culham Campus, Abingdon OX143DB, United Kingdom*
[3] *Max-Planck-Institut für Plasmaphysik, Boltzmannstr. 2, 85748 Garching, Germany*
[4] *Laboratory for Plasma Physics, ERM/KMS, B-1000 Brussels, Belgium*
[5] *See the author list of C.F. Maggi et al 2024 Nucl. Fusion* ***64*** *https://doi.org/10.1088/1741-4326/ad3e16*
[6] *See the author list of N. Vianello et al 2026 Nucl. Fusion in press https://doi.org/10.1088/1741-4326/ae71ec*

Introduction

Tritium-rich regimes based on the hybrid scenario [Maslov 2023] are complementary to 50/50 deuterium/tritium plasma mixture regimes [Hobirk 2023]. While not intended as operating scenarios for large-scale fusion devices, they enabled the record fusion energies achieved during the two most recent JET D-T campaigns: 59 MJ in DTE2 (2021) [Maggi 2024] and 69 MJ in DTE3 (2023) [Kappatou 2025]. Experimental evidence indicates that the presence of internal transport barriers (ITBs) significantly influences tungsten transport in T-rich regimes [Maslov 2026]. We present a qualitative analysis of a radial correlation reflectometry (RCR) dataset, focusing on DTE2 and DTE3, aiming to provide insight into turbulence behavior in high-performance T-rich and related hybrid pulses, with emphasis on the role of ITBs and their relationship to tungsten accumulation.

Results and Discussion

Density fluctuations were measured using a fixed RCR configuration, thus ensuring comparability across pulses. The microwave cutoff positions are determined from the electron density obtained via profile-reconstruction reflectometry and the magnetic field magnitude derived from equilibrium reconstruction. The two X-mode reflectometers operate in the F band (90 – 140 GHz) with typical density and toroidal magnetic field values $n_e \sim 8\times10^{19}$ m^{-3} and $B_t = 3.86$ T, respectively. Under these conditions, the slower (master) channel scans radially by increasing its frequency in 3 GHz steps, moving from the edge pedestal ($R \approx 3.8$ m) towards the plasma core ($R \approx 3.25$ m). At each master step, the faster-hopping (slave) channel increments its frequency in five successive 500 MHz steps from a initial offset of 250 MHz above the master frequency, yielding up to six valid measurements of the master-slave coherence, γ. In most cases, these are sufficient to determine the

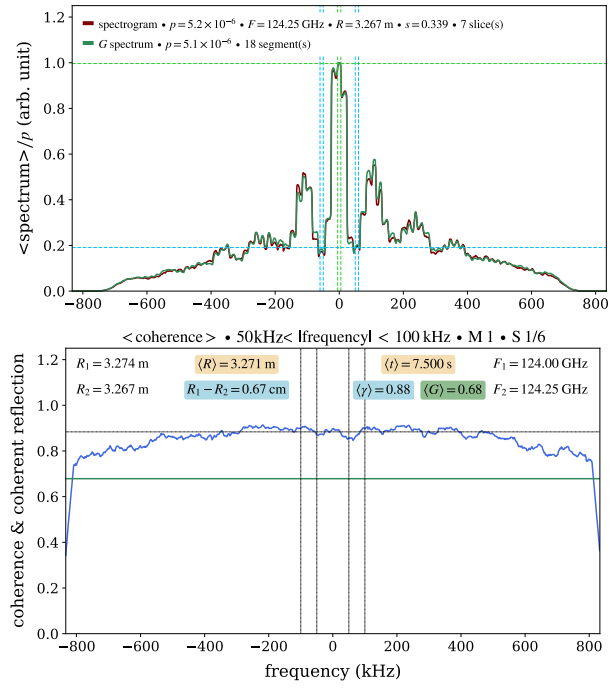

Figure 1. RCR spectrum from channel 2 (slave) and calculation of G for pulse 104520. The coherence γ is computed from spectra of both channels.

radial correlation length, L_{RCR}, which is obtained as the 1/e decay length of an exponential fit to the measured dependence of γ on the radial separation between the cutoff positions of the two microwave beams [Figueiredo 2008]. The relatively large frequency spacing of the slave channel can introduce a significant error in the estimation of the smallest L_{RCR} values. In addition to the evaluation of L_{RCR}, spectral characteristics are examined, and the coherent reflection of the microwave beams is calculated, as illustrated in Figure 1. Coherent reflection is herein defined as a normalized quantity, $0 \le G \le 1$, which represents the relative weight of the DC component in RCR spectra, corresponding to the specular component of microwave reflection. For that purpose, the mean spectral power within the –5 kHz to +5 kHz frequency band, P_{DC}, is compared with the mean power over a 10 kHz frequency interval within the 30 – 60 kHz range, typical of density fluctuations, $P_{\delta n}$, leading to the definition $G = (P_{DC} - P_{\delta n}) / (P_{DC} + P_{\delta n})$. Lower values of G are associated with higher density fluctuation levels, which in turn have an impact on L_{RCR}, by reducing its value relative to the correlation length of the density fluctuations, $L_{\delta n}$ [Kramer 2003].

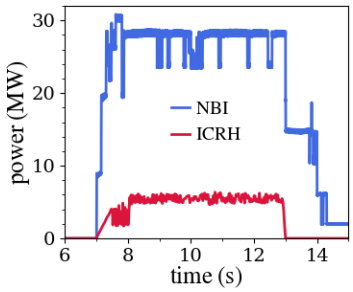

Figure 2. External heating power in pulse 104675.

In general, the dataset is characterized by good measurement quality, with RCR spectra showing a broad gaussian shape and a peaked DC component. Visual inspection of the spectra reveals peaks in the 100 – 200 kHz frequency range with characteristic widths of the order of 50 kHz, characteristic of quasi-coherent modes (Figure 1), although the trapped-electron mode is not expected to be dominant in these plasmas [Citrin 2017]. These features, which are absent from magnetic pickup signals, are observed in all T-rich pulses. They are localized within the radial interval 3.2 m < R < 3.3 m. Less frequently, similar peaks are also detected in the edge pedestal region. The coherence between the two RCR channels is high and progressively decreasing as the separation in frequency, and cutoff layer, increases. The microwave beams penetrate into the plasma core, reaching as far as the ITB foot in most pulses, and exceptionally extending into the ITB. The timing of the external heating power, a DTE3 example of which is shown in Figure 2 for a

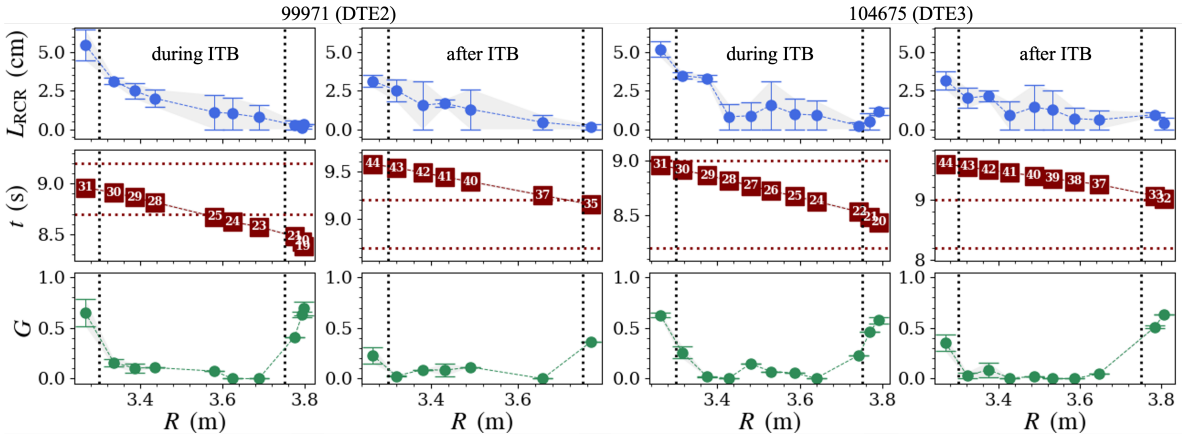

Figure 3. L_{RCR} and G comparison between the ITB and post-ITB phases, in DTE2 and DTE3 T-rich pulses. The positions of the pedestal top and of the ITB foot are marked, as well as the beginning and end of the ITB phase. Measurements are not simultaneous across radius: the RCR cutoff position progressively shifts towards the core as the master microwave frequency increases.

T-rich pulse, is the same for all the analyzed pulses [Maslov 2026]. In DTE2, 30 MW of Neutral Beam Injection (NBI) power were applied, starting at 7 s, along with 3.8 MW of Ion Cyclotron

Resonance Heating (ICRH), leading to a 5 s period of maximum fusion power, approximately from 8 s to 13 s [Maslov 2026]. During the 8.1–8.5 s interval, a transient ITB begins to develop at the $q = 1$ flux surface, terminating around 9 s. The presence of the ITB, associated with anomalous transport reduction and higher pressure at the plasma core, seems to have had little impact on total fusion power, its main effect being enhanced tungsten accumulation and eventual plasma degradation [Maslov 2026], as neoclassical transport within the ITB facilitates the accumulation of high Z impurities [Dux 2004]. ITB characterization during DTE2 was limited since the density and temperature profiles from the high-resolution Thomson scattering (HRTS) diagnostic did not allow full access to the plasma core, which became possible in DTE3.

Three T-rich pulses were performed in DTE3, essentially reproducing the DTE2 scenario with increased ICRH coupled power (up to 5.5 MW). The strategy was to enhance turbulent transport, thereby mitigating tungsten accumulation, which indeed proceeded at a lower rate than in DTE2, but could not be entirely suppressed. In particular, fusion power did not remain stationary for 5 s in the DTE3 record-energy pulse, 104522 (30 MW of NBI power), due to tungsten accumulation. The comparison with DTE2 is restricted to the stationary pulses, 104520 and 104675 (28 MW of NBI power), due to a malfunction of the RCR slave channel in 104522.

A general trend is observed across the dataset, which can be seen in Figure 3. As expected, G is relatively high within the pedestal, consistent with turbulence reduction inside the edge transport barrier. Regarding the ITB, the RCR signature is similar in DTE2 and in DTE3: during the interval in which the ITB is established, L_{RCR} and G are relatively high at the ITB foot region, compared to the mid-radius region. While the higher G indicates a lower turbulence level, the behavior of L_{RCR} at the ITB foot may be attributed to its nontrivial dependence on both the level and the correlation length of density fluctuations, which tend to increase L_{RCR}, and on flow shear, which tends to decrease it. In periods without an ITB, L_{RCR} and G still show a gradual increase inwards from the top of the edge pedestal to the ITB foot, consistent with reduced density fluctuations towards the plasma core [Fonck 1993, White 2008].

In general, RCR access to the ITB was limited to the ITB foot region. However, in pulse 99950, a 50/50 D/T hybrid plasma at a reduced magnetic field $B_t = 3.4$ T, the microwaves reached the interior of the ITB, as seen in Figure 4. In this case, L_{RCR} decreases significantly 10 – 20 cm inwards from the ITB foot, while G remains high. This radial variation can be explained by a decrease of the turbulence level and correlation length $L_{\delta n}$ within the ITB. While this single additional data point should be interpreted with caution, the result nevertheless suggests consistent behavior at the ITB foot and within the ITB, as it terminates, in both L_{RCR} and, in particular, G.

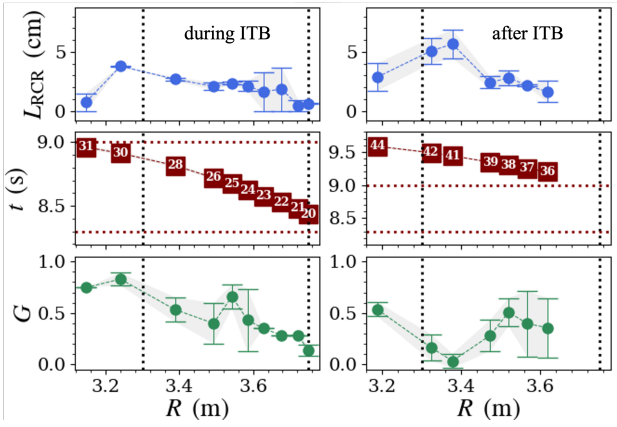

Figure 4. Analysis of the 50/50 D/T hybrid pulse 99950 at $B_t = 3.4$ T, showing the behavior of L_{RCR} and G within the ITB, and an increase in L_{RCR} after the ITB collapses.

Figure 3 presents a comparison between two T-rich pulses: 99971 from DTE2 and 104675 from DTE3, the latter featuring a 40% higher ICRH power. The behavior of L_{RCR} and G is very similar in both cases, particularly at the ITB foot region. Nevertheless, the decrease in G around $R \approx 3.3$ m, associated with the collapse of the ITB,

appears to be slightly less pronounced in the DTE3 pulse. If confirmed, such an effect could suggest that the rise in core turbulence relative to the preceding ITB phase is somewhat weaker in DTE3 than in DTE2, indicating greater resilience of the plasma core following ITB termination. Although such an effect might, in principle, improve fusion efficiency, the brief duration of the ITB would limit the extent of this improvement. This effect could not be confirmed in pulse 104520, which could be due to the lower ICRH power (4.8 MW versus 5.5 MW in 104675).

The RCR analysis of two 50/50 DT hybrid pulses from DTE2, 99950 and 99951, revealed a different behavior from the T-rich pulses. Following the collapse of the ITB, instead of an L_{RCR} decrease at the ITB foot, as observed in T-rich pulses, in these hybrid pulses L_{RCR} increases, as seen in Figure 4. As for G, it does decrease but remains relatively high compared with T-rich pulses, which, together with the $L_{\delta n}$ increase due to flow shear reduction, contributes to explain the difference in the behavior of L_{RCR}. This difference is indicative of a relatively quieter core in the 50/50 DT hybrid pulses, in terms of the amplitude of the density fluctuations.

Summary

The analysis of the RCR dataset from DTE2 and DTE3 is constrained by limited access to the ITB region. Nevertheless, it shows a clear reduction of density fluctuations at the foot of the ITB, both for T-rich and 50/50 DT hybrid pulses, which is consistent with the reduction of turbulent transport [Maslov 2026]. This reduction has been observed both in DTE3 and in DTE2, for which a direct identification of the ITB in HRTS profiles had not been possible [Maslov 2023, Maslov 2026]. The T-rich pulses show higher turbulence levels after the ITB ends than the 50/50 DT hybrid pulses. RCR analysis revealed no significant differences in ITB behavior between T-rich pulses in DTE2 and DTE3. The possibility that the increase in core turbulence associated with ITB termination is less pronounced in DTE3 T-rich pulses than in comparable DTE2 pulses, suggested only weakly by one DTE3 pulse, has not been confirmed across the dataset.

Acknowledgments

This work has been carried out within the framework of the EUROfusion Consortium, funded by the European Union via the Euratom Research and Training Programme (Grant Agreement No. 101052200 – EUROfusion). Views and opinions expressed are however those of the author(s) only and do not necessarily reflect those of the European Union or the European Commission. Neither the European Union nor the European Commission can be held responsible for them. IPFN activities were supported by FCT – Fundação para a Ciência e Tecnologia, I.P. through project UID/50010/2025 (https://doi.org/10.54499/UID/50010/2025).

References

[Maslov 2023] M. Maslov *et al* Nucl. Fusion **63** (2023) 112002.

[Hobirk 2023] J. Hobirk *et al* Nucl. Fusion **63** (2023) 112001.

[Maggi 2024] C.F. Maggi *et al* Nucl. Fusion **64** (2024) 112012.

[Kappatou 2025] A. Kappatou *et al* Plasma Phys. Control. Fusion **67** (2025) 045039.

[Maslov 2026] M. Maslov *et al* "Insights of the JET high fusion power scenario in the final DT campaign" to be submitted to Nucl. Fusion.

[Figueiredo 2008] A. Figueiredo *et al* Rev. Sci. Instrum. **79** (2008) 10F107.

[Kramer 2003] G.J. Kramer, R. Nazikian, and E. Valeo, Rev. Sci. Instrum. **74** (2003) 1421.

[Citrin 2017] J. Citrin *et al* Plasma Phys. Control. Fusion **59** (2017) 064010.

[Dux 2004] R. Dux *et al* Nucl. Fusion **63** (2004) 260.

[Fonck 1993] R.J. Fonck *et al* Phys. Rev. Lett. **70** (1993) 3736.

[White 2008] A.E. White *et al* Rev. Sci. Instrum. **79** (2008) 103505.